https://doi.org/10.5194/egusphere-2023-518
Preprint. Discussion started: 11 April 2023

On the relationship between mesoscale cellular convection and meteorological forcing: Comparing the Southern Ocean against the North Pacific

Francisco Lang[1], Steven T. Siems[1,2], Yi Huang[3,4], and Luis Ackermann[5]

[1]School of Earth, Atmosphere and Environment, Monash University, Melbourne, Victoria, Australia.
[2]Australian Research Council Securing Antarctica's Environmental Future (SAEF), Melbourne, Victoria, Australia.
[3]School of Earth Sciences, The University of Melbourne, Melbourne, Victoria, Australia.
[4]Australian Research Council Centre of Excellence for Climate Extremes (CLEX), Melbourne, Victoria, Australia.
[5]Australian Bureau of Meteorology, Melbourne, Victoria, Australia

Correspondence: Francisco Lang (francisco.lang@monash.edu)

Abstract. Marine atmospheric boundary layer (MABL) clouds cover vast areas over the ocean and have important radiative effects on the Earth's climate system. These radiative effects are known to be sensitive to the local organization, or structure, of the mesoscale cellular convection (MCC). A convolution neural network model is used to identify the two ideal classes of MCC clouds, namely open and closed, over the Southern Ocean (SO) and Northwest Pacific (NP) from high-frequency geostationary Himawari-8 satellite observations. The results of the climatology show that MCC clouds are roughly distributed over the midlatitude storm tracks for both hemispheres, with peaks poleward of the 40° latitude. Open MCC clouds are more prevalent than closed MCC in both regions. An examination of meteorological forcing associated with open and closed MCC clouds is conducted to illustrate the influence of large-scale meteorological conditions. We establish the importance of the Kuroshio western boundary current in the spatial coverage of open and closed MCC across the NP, presumably through the supply of strong heat and moisture fluxes during marine cold air outbreaks events. For both regions, closed MCC cloud are more frequent at higher static stability than on air-sea temperature difference, opposite to the open MCC cloud behavior. The diurnal cycle reveals a pronounced daily cycle in the frequency of occurrence of closed MCC over the SO, while the NP closed MCC daily cycle is less noticeable.

1 Introduction

Marine atmospheric boundary layer (MABL) clouds have a significant contribution to the energy budget over the oceans (Trenberth and Fasullo, 2010), covering nearly 25% of the marine surface (Wood, 2012). Small changes in the spatial distribution or physical properties of these clouds are required to produce important radiative effects in the high and midlatitudes (Bodas-Salcedo et al., 2016). Given the remote location of these clouds, satellite observations have been indispensable for advancing

https://doi.org/10.5194/egusphere-2023-518
Preprint. Discussion started: 11 April 2023

our understanding of them. The first satellite observations in the early 1960s (e.g., Agee and Dowell, 1974; Atkinson and Zhang, 1996) revealed that these shallow clouds commonly take the form of open or closed mesoscale cellular convection (MCC), which are defined by distinct patterns of organization. These clouds are particularly import to the climate, as they help regulate both the shortwave and long-wave fluxes into and out of the ocean, as well as sensible and latent heat fluxes. For example, closed MCC clouds over the Southern Ocean (SO) have been found to have on average a higher albedo than open MCC clouds for the same cloud fraction, which can drive changes in the cloud radiative effect up to 39 W m^{-2}, depending on season and cloud phase (Danker et al., 2022; McCoy et al., 2017). In a case study over the SO, (Lang et al., 2021) observed strong cold pools formed under open MCC downdrafts, helping decouple MABL. Wood and Hartmann (2006) first developed a cloud classification algorithm to classify low-level clouds scenes from satellite observations over the eastern subtropical Pacific Ocean into four categories based on the level of cellularity and mesoscale organization: open, closed, cellular but disorganized MCCs and no MCC present. Their method was based on the training of a two-layer neural network on probability distribution functions and 2-D power spectra of liquid water path; their analysis, however, was limited to only 2 months of data over a region limited to warm clouds.

More recent investigations of MCC cloud classification have more comprehensively examined the Earth's oceans using machine learning (e.g., Rampal and Davies, 2020; Watson-Parris et al., 2021; Yuan et al., 2020), confirming that these various MCC cloud formations dominate are most common in the midlatitude storm tracks (Lang et al., 2022; Muhlbauer et al., 2014). They are commonly associated with the cold air sector of extra-tropical cyclones and the ensuing marine cold air outbreaks (MCAO) (Fletcher et al., 2016b) where cold polar air masses advect over warmer waters at lower latitudes (Abel et al., 2017; Fletcher et al., 2016a). MCAO events are characterized by strong latent and sensible heat fluxes that drive the MABL convection and the distinct mesoscale organization of these clouds. Strong MCAOs are characterized by greater cloud fraction and optical thickness than weak ones, resulting in a greater shortwave cloud radiative effect (Fletcher et al., 2016b). Fletcher et al. (2016a) investigated MCAOs in both hemispheres and found that they are more vigorous and more frequent in the Northern Hemisphere (NH) than the Southern Hemisphere (SH). Lang et al. (2022) built a climatology of open and closed MCC over the Australian sector of the SO using geostationary satellite data from Himawari-8 and a convolutional neural network. An advantage of this methodology was that spatial inhomogeneities, from SST gradients to orography, became apparent. They showed that the SST gradient at the SO polar ocean front was spatially correlated with the distribution of MCC clouds, establishing a southern boundary over the SO. Further their climatology found that open MCC were more frequent than closed MCC, and they are largely uniformly distributed over the SO storm track across the midlatitudes. Taking advantage of the high temporal resolution of Himawari-8, they found that the closed MCC have a pronounced daily cycle, which is most intense during the summer months.

Comparisons of the mid-latitude storm track between the two hemispheres have found a variety of differences beyond MCAOs. Huang et al. (2015) used reanalysis datasets and A-Train observations to show differences in the storm-track cloud properties. They found that the North Atlantic has a stronger seasonality in cloud properties than the SO. In summer, boundary layer cloud heights between the two region are comparable, while the wintertime North Atlantic is dominated by higher boundary layer clouds than the SO. With CloudSat/CALIPSO observations, Muhlbauer et al. (2014) showed that the seasonal

https://doi.org/10.5194/egusphere-2023-518
Preprint. Discussion started: 11 April 2023

cycle of low-level cloud fraction peaks during boreal summer in the midlatitude storm track regions of the North Atlantic and North Pacific while a seasonal cycle is almost absent in the SO. MCC clouds systems have also shown difference between the NH and the SH environments. McCoy et al. (2017) used Moderate Resolution Imaging Spectroradiometer (MODIS) data to demonstrate that surface fluxes and inversion strength are both important for these cloud types; however, over the midlatitudes, surface forcing appears to be much more important to closed MCC in the NH than in the SH. This surface forcing undergoes a much stronger seasonal cycle over the NH reflecting the larger cycle in the temperature of terrestrial air masses in the NH. Another substantial difference between the NH and the SH is aerosol characteristics, which can alter cloud structure, microphysical, and radiative properties. For example, satellite retrievals of cloud-top phase indicate that supercooled liquid water is more prevalent over the SO than at equivalent latitudes in the NH (Choi et al., 2010; Hu et al., 2010; Morrison et al., 2011). Using MODIS observations, Huang et al. (2016) also found that the average cloud droplet number concentration is substantially greater over the North Pacific than the mid-latitude SO.

In this work, we extend the climatology of Lang et al. (2022) to the Northwest Pacific (NP), which is also covered by Himawari-8 observations. The objective of this study is to investigate the differences between open and closed MCC cloud distributions and their relationship with meteorological forcing over the NP and the SO. First, we consider the estimated inversion strength (EIS, Wood and Bretherton, 2006) calculated from ERA5 reanalysis.

High EIS is associated with strong and low-lying inversions, trapping moisture within the MABL more efficiently and promoting greater cloud cover (e.g., Lang et al., 2018; Kawai et al., 2017). Naud et al. (2016) demonstrated that EIS is well correlated to cloud cover in dynamically active sectors after cold front passages. Next, we examine the relationship with respect to the MCAO index, M (Fletcher et al., 2016a), defined as the difference between the ocean potential skin temperature and the 800 hPa potential temperature. McCoy et al. (2017) found that the M index is a good predictor of MCC clouds organization in the extra-tropical oceans. Again, taking advantage of the geostationary platform our analysis focusses on differences between the NP and the SO.

2 Data and methodology

2.1 Data source and domain

The classification dataset used is derived from the Advanced Himawari Imager (AHI) on board the Himawari-8 geostationary meteorological satellite (Bessho et al., 2016). Himawari-8 was launched in July 2015 by the Japanese Meteorological Agency. Himawari-8 scenes and cloud products are available on the Japan Aerospace Exploration Agency (JAXA) P-Tree System. Himawari-8 provides a temporal resolution of 10 min and spatial resolutions ranging from 1 to 5 km. Hourly brightness temperature from infrared channel 11 (8.6 μm) at 5 km resolution in an orthogonal gridded projection was used for the model training and subsequent MCC climatology classification.

For this study, the analysis is based on 3 years (2016-2018) of Himawari-8 scenes from the SH region, (20-60° S, 80°E-160° W) which includes the SO and portions of the Pacific and Indian oceans, as well as scenes from the NP region (20-60° N, 80°E-160° W). Centered at 140.7° E the satellite covers the Asia-Oceania region. Both domains encompass the area of

https://doi.org/10.5194/egusphere-2023-518
Preprint. Discussion started: 11 April 2023

the storm tracks in the midlatitude that are directly associated with MCAOs. Reanalysis data are employed in this study to examine the large-scale meteorological forcing on MCC clouds. We used the the European Centre for Medium-Range Weather Forecasts (ECMWF) ERA5 reanalysis (Hersbach et al., 2020). Hourly data gridded to 0.75 × 0.75° grid boxes are used over the two regions between 2016 and 2018.

2.2 Cloud type classification

The Lang et al. (2022) classification scheme of MABL clouds is based on a hybrid convolutional neural network (CNN) model defined for the two primary classes of MCC clouds: open and closed. By default, the algorithm includes a third category called "other" that it is used for all other coverage including mid-, and high-level clouds, stratus, and disorganized MCC and even clear sky. Hourly brightness temperature at 5 km resolution from infrared channel 11 (8.6 μm) is used as the main input to train the CNN. To build up the labelled training data set, additional Himawari-8 channels and products were used as contextual information and filtering. A full description of the machine learning training and performance evaluation can be found in Lang et al. (2022). Examples of training samples for the three categories can be found in Fig. 2 of Lang et al. (2022). The classification algorithm developed in Lang et al. (2022) found an average precision of about 89 % across all categories. Open MCC had the lowest accuracy, most likely because it had the smallest training sample size. The largest source of uncertainty reported by Lang et al. (2022) was the difficulty to separate open from disorganized MCC, a challenge similarly discussed in Yuan et al. (2020).

An example of a classified image from Himawari-8 during the winter over the NP midlatitude is shown in Fig. 1. The scene shows a frontal band moving eastward followed by groups of open and closed MCC clouds in a post-frontal environment. Closed MCCs are primarily observed to the northwest of open MCCs.

2.3 Large-scale meteorological indices

Two meteorological indices are employed in our study, the Estimated Inversion Strength (EIS, Wood and Bretherton, 2006) and the MCAO index (M, Fletcher et al., 2016a), both representing different features of large-scale dynamic and thermodynamic influences on open and closed MCC cloud development. EIS is a measure of the strength of the boundary layer inversion, an indicator of the static stability of the lower atmosphere and is defined as follows:

$$EIS = LTS - \Gamma_m^{850}\,(z_{700} - LCL)\,, \tag{1}$$

where LTS is the lower tropospheric stability defined in (Klein and Hartmann, 1993), which is the difference in potential temperature between 700 hPa and the surface ($LTS = \theta_{700} - \theta_{surf}$). The variable Γ_m^{850} is the moist-adiabatic potential temperature gradient at 850 hPa; z_{700} is the altitude of the 700-hPa level, and LCL is the lifting condensation level. Figure 2 shows the frequencies of occurrence of the EIS estimated from the ERA5 reanalysis products between 2016 and 2018, for the region between 60° N-60° S and 80° E-160° W, which corresponds to the area of the Himawari-8 full disk. For both hemispheres, the highest EIS values are primarily observed over the subtropics and part of the midlatitude regions, with a local maximum over

https://doi.org/10.5194/egusphere-2023-518
Preprint. Discussion started: 11 April 2023

the southeastern Indian Ocean in the SH and over the Sea of Okhotsk in the NH. Both areas have been associated with high percentages of low-cloud fraction (Muhlbauer et al., 2014).

The MCAO index M is defined as the difference between the surface skin potential temperature and the 850-hPa potential temperature:

$$M = \theta_{SKN} - \theta_{850}, \tag{2}$$

Fletcher et al. (2016a, b) based the index M on the surface skin temperature and not the sea surface temperature (SST), to exclude areas of high sea ice cover. Fletcher et al. (2016a) used the potential temperature at 800 hPa, while Papritz et al. (2015) used 850-hPa potential temperature over the South Pacific. We tested both potential temperature levels and found that using the 800-hPa level produced far fewer MCAOs over the SO than using the 850-hPa level, which makes the 850-hPa potential temperature level a more appropriate value to compare the two regions. Following Fletcher et al. (2016a) we define MCAOs as contiguous oceanic regions where $M > 0$ K. Figure 2b shows the frequency of occurrence of M. The relative frequency was defined by dividing the amount of time where $M > 0$ by the extent of the full record.

For both hemispheres, MCAOs most often occur in areas with a strong SST gradient over the midlatitude (Figure 2c), most notably the Kuroshio region, east of Japan, with a frequency of 50%. This is consistent with the results found in Fletcher et al. (2016b) for M index using ERA-Interim data. The 3-yr mean SST composite is shown in Fig. 2c. In general, the SH SSTs are colder than the NH counterparts for the same latitude bands. Over the SO midlatitudes, the oceanic polar front is a pronounced feature, associated with the strongest meridional SST gradients. The full-year SST gradients in the NP ocean, on the other hand, are weaker.

3 Results

The period analyzed cover the hourly brightness temperature images from Himawari-8 between 2016 and 2018, for both the SO and NP regions. For this period, 25,494 images were processed and classified into each category (open MCC, closed MCC, and other) and $\sim$ 400 were used as the training data set (Lang et al., 2022). We note that the training data came from only over the SO. A visual inspection of cloud cover over the NH storm track confirmed that the algorithm was producing robust results for both hemispheres.

3.1 MCC climatology: North Pacific versus Southern Ocean

The annual frequency of occurrence of MCC clouds is defined as the number of times a cloud category is observed in a grid point divided by the total time (Figure 3). Results for the SO have previously been discussed in Lang et al. (2022). Focusing on the NP here, we observe peak frequencies of both open and closed MCC poleward of 40° N latitude with the peak in closed MCC being slightly closer to Asia ($\sim$ 160° E) than for the open MCC ($\sim$ 180° E). Strong gradients in the frequency of open MCC are apparent to be the north and south of this band of open MCC, with few present equatorward of 30° N and poleward

https://doi.org/10.5194/egusphere-2023-518
Preprint. Discussion started: 11 April 2023

of 55° N. A small local peak is also observed just to the east of the Tohoku Prefecture in Japan. Closed MCCs are located primarily at poleward of 40° N with small peaks in the Sea of Japan, the Sea of Okhotsk and the Bering Sea. The frequency exceeds 20 % in a band across much of the SO midlatitudes compared to 13 % across the midlatitude band across the NP. Overall, we observe the peak frequency of open MCC to be much greater over the SO ($\sim$ 25 %) than over the NP ($\sim$ 16 %). Conversely for closed MCC, we observe little difference in the peak frequency over the SO (11 %) and the NP ($\sim$ 13 %), but this overlooks an important difference between the hemispheres. Over the SO, the peak is over the southeast Indian Ocean off the coast of southwest Western Australia. This is a region dominated by sub-tropical subsidence (Atkinson and Zhang, 1996) rather than the SO storm track, and is also influenced by the colder SST due to the Western Australian current. Looking at the higher latitude band (40 - 60°), we find more closed MCC over the NP than the SO. Closed MCC is evident to the top of the domain over the NP, but if relatively sparse at high latitudes of the SO, poleward of the ocean polar front.

We can look back at the spatial relationship between the annual frequency of open and closed MCC (Figure 3) against the EIS, M index and SST gradient (Figure 2, top row). As discussed in Lang et al. (2022), the frequency of open MCC is loosely spatially correlated with the SST gradient across the midlatitudes of the SO. We see a similar relationship across the NP following the Kuroshio current. Spatially, the magnitude of the M index does not appear to be as highly correlated with the frequency of open MCC. Arguably, the magnitude of the M index does bear a relationship to the frequency of closed MCC. Looking at the spatial distribution of the static stability (Fig. 2a), EIS is spatially correlated with the peaks of closed MCC clouds in both hemispheres (Fig. 3b), but not the open MCC.

The relationship between both large-scale meteorological parameters (M index and EIS) and each MCC category is graphically shown with two-dimensional histograms of M versus EIS (Fig. 44). Each two-dimensional histogram is calculated using a composite of the MCC clouds identified for each region. The highest MCC frequencies occurs for M index values between -2 and 5 K for both regions. The open MCC frequency in the NP is characterized by the highest M index values with a difference of 3 K higher compared to the maximum frequency of open MCC over the SO, consistent with stronger marine cold air outbreaks in the NH than in the SH (Fletcher et al., 2016a). Closed MCCs have a weaker relationship with M, depending more strongly on EIS. The most pronounced difference between open and closed MCC is found for EIS. Figure 4 shows that closed MCC clouds are more frequently associated with larger EIS values, opposite to the open MCC cloud behavior. On average, EIS for closed MCC is 5 K larger than open MCC values, ranging from about 5 to 10 K. For both categories, the SO clouds have a better relation against EIS compared to the NP.

3.2 Summer and Winter Seasons

As previously discussed, these midlatitude storm tracks undergo a strong seasonal cycle, particularly across the NP where the storm track largely collapses over the summer (Hoskins and Hodges, 2005). As such, it is worthwhile to extend our analysis to the winter and summer seasons, separately (Figure 5). In general, open MCC exhibits a considerable seasonal difference between summer and winter. In both regions, the maximum frequency of occurrence for open MCC clouds is found during the winter season, with values of 40 % for the NP and 27 % for the SO. During summertime, a considerable reduction in the frequency of occurrence for open MCCs is observed for both regions, especially for the NP, with maximum values of 13

https://doi.org/10.5194/egusphere-2023-518
Preprint. Discussion started: 11 April 2023

% and 20 % (NP and SO, respectively). This strong seasonality in the open MCC frequency can be related to the frequency of occurrence of marine cold air outbreaks as observed in Fig. 2e and 2h and Table 1. The presence of cold air outbreaks is considerable higher during wintertime, especially for the NP, reaching frequencies of occurrence of 90 % over this region. Figure 2e shows that during summer it is still possible to detect marine cold air outbreaks over the SO, in contrast to the NP.

Compared to open MCC, the frequency of closed MCC shows less interseasonal variability (Fig. 5b,d), with peaks slightly higher during summer, 15 % and 13 % for the NP and SO, respectively. During this season, the frequency peaks move poleward along with the storm track for both hemispheres. For both seasons, the southeastern Indian Ocean (SO region) and east of Japan (NP region) are the areas with the highest frequency of occurrences for closed MCCs. While the presence of marine cold air outbreaks is also a factor in the development of closed MCC (Fig. 6), Fig. 2d and 2g show that the EIS is a more relevant factor for development of closed MCCs compared to open MCCs, displaying a better alignment with the peaks in both hemispheres and for both seasons. The distribution of the summer peaks of MCC closed clouds occurrence for both hemisphere (except for the values off the Russian coast over the Sea of Okhotsk) is correlated with higher EIS, which is consistent with Fig. 6, where high EIS are associated with higher presence of closed MCC clouds.

The seasonal differences in both EIS and M indices and their influence on MCC clouds may largely be explained by the large-scale dynamic, thermodynamic influences of the SST and the fact that land masses represent a smaller surface area in the SO compared to the NP. The NP has a large seasonal cycle in SST (Fig. 2g and 2i), particularly at the high latitudes, where the ocean basin is relatively shallow. Winter season shows the extension of colder SST towards the equator, which explain the higher frequency of open MCCs in both hemispheres. In turn, closed MCCs frequency of occurrence at lower latitudes is higher that poleward during wintertime.

3.3 Diurnal Cycle

The diurnal cycle of the MCC frequencies is calculated over boxes of 10 × 10°, center at 40° N, 170° W (NP) and 45° S, 130° W (SO) (Fig. 7). Comparing the annual means between NP and SO, closed MCC over the SO exhibits the most pronounced daily cycle with higher frequencies at night, and a peak of 13 % at 07:00 local standard time (LST) and a minimum at 15:00 LST (6.2 %, Fig. 7b), with a range of the cycle of $\sim$ 7 %. In contrast, closed MCC over the NP exhibits a less noticeable diurnal cycle, with a peak of 21 % at 02:00 LTS and a range of the cycle of $\sim$ 4 % (Fig. 7a). It is also noticeable that the standard deviation of the open MCC frequency shows a higher variability compared to closed MCC clouds over the SO, while the standard deviations for open and closed MCC frequencies show similar variability over the NP. Looking at the summer and winter means, a closed MCC diurnal cycle was identifiable for both seasons over the SO, being most intense during the summer months (December–February), with a range of the cycle of $\sim$ 7 %. During wintertime, a closed MCC diurnal cycle in the NP is identifiable as well, while a diurnal cycle in the summertime NP (June-August) is almost absent. For closed MCCs, the seasonal standard deviations show larger differences between both seasons, with a lower variability during summer and higher during winter for both regions. In contrast, the seasonal standard deviations of the open MCC frequency is lower during summer over the NP and the SO. A contrast between both regions is that the most pronounced daily cycle for closed MCCs is in opposite season, summer over the SO ($\sim$ 4 % of diurnal range), and winter over the NP ($\sim$ 5 % of diurnal range).

https://doi.org/10.5194/egusphere-2023-518
Preprint. Discussion started: 11 April 2023

The annual diurnal cycle of open MCC is less distinct for both regions, with maximums of 29 % at 11:00 LST and 23 % at 21:00 LTS, NP and SO respectively. The standard deviation for open MCC shows a large variability during the day for both regions. Compared to the SO closed MCC, open MCC shows more variability throughout the day. During wintertime, the open MCC occurrence over the NP shows a slightly more noticeable daily cycle with a peak of 38 % at 11:00 LTS (Fig. 7e) and with the highest variability for both regions and seasons ($\sim$ 13 %). The open MCC occurrence shows higher frequencies and variability during winter that summer in both regions.

4 Discussion and conclusions

In Lang et al. (2022), a CNN model was developed to identify and classify open and closed MCC clouds from high-frequency geostationary Himawari-8 satellite observations over the SO. Here, this analysis is extended to the North Pacific to identify differences in the organization of MABL clouds between the hemispheres. The inputs to the CNN model consist of hourly brightness temperature from AHI Himawari-8 during the period 2016-2018 for the regions defined as SO (20-60° S, 80°E-160° W) and NP (20-60° N, 80°E-160° W). Two large-scale meteorological parameters are chosen to study their influences on the MCC distributions: EIS and MCAO index (M).

The climatology for both regions showed that MCC clouds are roughly distributed over the midlatitude storm tracks of both hemispheres, with peaks poleward of the 40° latitude. The distribution of MCC clouds is consistent with their large contributions to shallow clouds that can also be found in the midlatitude as observed by CloudSat/CALIPSO (Muhlbauer et al., 2014). Our results found that open MCC clouds are the most prevalent type of MABL cloud in both regions and that the highest frequencies are observed over the SO. The local frequency maximums of open MCC are 25 % for the SO and 16 % for the NP. For closed MCCs, they are represented by lower frequencies compared with open MCCs, with a frequency rather comparable between both regions (local maximums of 12 % and 14 % for the SO and NP respectively). The annual mean frequencies in Fig. 2b show that closed MCCs are more frequently found at higher latitudes over the NP, consistent with Rampal and Davies (2020), whereas these clouds are less prevalent at high latitudes of the SO. Truong et al. (2020) found that across the SO storm track and higher latitudes, the presence of multilayer clouds is a common feature, which might explain a low frequency of occurrence for SO closed MCCs (Mace et al., 2009).

Previous studies have linked the marine cold air outbreaks to the presence of MCC clouds over midlatitude (e.g., McCoy et al., 2017). This is mainly due to the enhanced surface forcing when these cold air masses are advected over warmer oceans, which increases the turbulent heat flux (latent plus sensible heat flux) and moisture from the surface into the marine boundary layer, driving the formation of MABL clouds (Abel et al., 2017; Fletcher et al., 2016b; Kolstad et al., 2009). The presence of marine cold air outbreaks for the analyses period is higher over the NP, with a peak frequency of occurrence of around $\sim$ 50 % in some areas, highlighting the current the Kuroshio region and its western boundary current (Fig. 2b). Over this region, open MCC clouds were often associated with stronger cold air outbreaks as measured by M index value (Fig. 4), with values on average 3 K higher for open MCCs that the SO. Considering both large-scale meteorological parameters, the two-dimensional composite histograms of M index and EIS (Fig. 4) show that both low static stability and strong surface forcing favor open

https://doi.org/10.5194/egusphere-2023-518
Preprint. Discussion started: 11 April 2023

MCC clouds. While closed MCC cloud are more frequent at a weaker M index, depending more strongly on EIS than on air-sea temperature difference, opposite to the open MCC cloud behavior. For closed MCCs a distinction between the two regions is also observed, the SO closed MCCs are associated with higher static stability compared with the NP region, which is consistent with Muhlbauer et al. (2014), where they found lower annual means of EIS for the NP. In addition, we noted that over the SO, the spatial correlation between closed MCC and high static stability is stronger over the sub-tropical southeastern Indian Ocean, while over the NP this correlation is associated with the storm track.

The seasonality of open MCC clouds (Fig. 5) is particularly strong, consistent with their relationship to marine cold air outbreaks (Fig. 2). In general, the frequency of open MCCs is higher over the NP than their SO counterparts during the respective winter. This larger seasonal difference between NP and SO is observed for both open and closed MCC, showing a strong relationship to the SST gradients, where the NH mean SSTs during winter are notably colder than the NH mean SSTs in summer, such that the seasonal difference is larger for the NH than the SH. In Addition, the difference in the landmass between both regions also influences the ocean-atmosphere interaction. The spatial distribution of the M index (Fig. 2) does not align strongly with the maximum occurrence of open MCC, especially over the NP during winter. The M index peaks closer to the Asian land mass. An explanation might be that very strong air-sea temperature difference leads to rapid convection that does not necessarily produce well-formed open cells. Despite this spatial misalignment, the two-dimensional composite histograms [both annual (Fig. 4) and by season (Fig. 6)] suggest a relationship between them. On the other hand, the seasonal differences in the EIS are consistent with Muhlbauer et al. (2014), where the annual cycle is found to be stronger over the NP as observed in Fig. 2. However, during both seasons, closed MCC clouds are positively correlated with EIS compared with open MCC clouds (Table 1). This high correlation between closed MCCs and the static stability is also observed in the spatial distribution throughout the year over both regions. The maximum of closed MCC clouds frequencies is aligned with the EIS maxima.

The analysis of the diurnal cycle of both MCC morphologies over both regions showed that the frequency of occurrence of closed MCC exhibits a distinctive daily cycle over the SO, while the NP closed MCC daily cycle is less noticeable. A maximum during the nighttime for closed MCC clouds has been particularly associated to the absence of solar forcing, where the marine boundary layer can become well mixed, and the cloud deck commonly thickens with the renewed access to moisture from the ocean surface (Minnis and Harrison, 1984; Nicholls, 1984). We also observed that the daily cycles have a maximum amplitude in different seasons depending on the region, over the SO the most pronounced daily cycle for closed MCCs is during warmer months, while over the NP is during winter.

The current CNN model has demonstrated overall a good performance over both regions. Future work will be extended to other machine learning techniques and the inclusion of more categories such as disorganized MCC, no MCC low-level clouds and clear sky. In addition to understanding the role of large-scale environmental conditions such as M and EIS, we will focus particularly in studying how the spatial organization of MCC clouds contributes to the daily cycle of shallow convection and precipitation.

Code availability. The code related to this article is available online at: https://doi.org/10.5281/zenodo.5657269

https://doi.org/10.5194/egusphere-2023-518
Preprint. Discussion started: 11 April 2023

Data availability. All Himawari-8 data can be accessed using the following public website: https://www.eorc.jaxa.jp/ptree/index. html (Japan Meteorological Agency, 2023).

Author contributions. FL performed the data analysis and wrote the article with the support of SS. FL and LA implemented the method to train the network model. All authors contributed to the discussion of the results and editing of the manuscript.

Competing interests. The authors declare that they have no conflict of interest.

Acknowledgements. Steven Siems is supported by Securing Antarctica's Environmental Future (SAEF), a Special Research Initiative of the Australian Research Council (SRI20010005).

https://doi.org/10.5194/egusphere-2023-518
Preprint. Discussion started: 11 April 2023

References

Abel, S. J., Boutle, I. A., Waite, K., Fox, S., Brown, P. R., Cotton, R., Lloyd, G., Choularton, T. W., and Bower, K. N.: The role of precipitation in controlling the transition from stratocumulus to cumulus clouds in a Northern Hemisphere cold-air outbreak, Journal of the Atmospheric Sciences, 74, 2293–2314, https://doi.org/https://doi.org/10.1175/JAS-D-16-0362.1, 2017.

Agee, E. and Dowell, K.: Observational studies of mesoscale cellular convection, Journal of Applied Meteorology and Climatology, 13, 46–53, https://doi.org/https://doi.org/10.1175/1520-0450(1974)013<0046:OSOMCC>2.0.CO;2, 1974.

Atkinson, B. W. and Zhang, J. W.: Mesoscale shallow convection in the atmosphere, Reviews of Geophysics, 34, 403–431, https://doi.org/https://doi.org/10.1029/96RG02623, 1996.

Bessho, K., Date, K., Hayashi, M., Ikeda, A., Imai, T., Inoue, H., Kumagai, Y., Miyakawa, T., Murata, H., Ohno, T., et al.: An introduction to Himawari-8/9—Japan's new-generation geostationary meteorological satellites, Journal of the Meteorological Society of Japan. Ser. II, 94, 151–183, https://doi.org/https://doi.org/10.2151/jmsj.2016-009, 2016.

Bodas-Salcedo, A., Hill, P., Furtado, K., Williams, K., Field, P., Manners, J., Hyder, P., and Kato, S.: Large contribution of supercooled liquid clouds to the solar radiation budget of the Southern Ocean, Journal of Climate, 29, 4213–4228, https://doi.org/https://doi.org/10.1175/JCLI-D-15-0564.1, 2016.

Choi, Y.-S., Ho, C.-H., Kim, S.-W., and Lindzen, R. S.: Observational diagnosis of cloud phase in the winter Antarctic atmosphere for parameterizations in climate models, Advances in Atmospheric Sciences, 27, 1233–1245, https://doi.org/https://doi.org/10.1007/s00376-010-9175-3., 2010.

Danker, J., Sourdeval, O., McCoy, I. L., Wood, R., and Possner, A.: Exploring relations between cloud morphology, cloud phase, and cloud radiative properties in Southern Ocean's stratocumulus clouds, Atmospheric Chemistry and Physics, 22, 10 247–10 265, https://doi.org/https://doi.org/10.5194/acp-22-10247-2022, 2022.

Fletcher, J., Mason, S., and Jakob, C.: The climatology, meteorology, and boundary layer structure of marine cold air outbreaks in both hemispheres, Journal of Climate, 29, 1999–2014, https://doi.org/https://doi.org/10.1175/JCLI-D-15-0268.1, 2016a.

Fletcher, J. K., Mason, S., and Jakob, C.: A climatology of clouds in marine cold air outbreaks in both hemispheres, Journal of Climate, 29, 6677–6692, https://doi.org/https://doi.org/10.1175/JCLI-D-15-0783.1, 2016b.

Hersbach, H., Bell, B., Berrisford, P., Hirahara, S., Horányi, A., Muñoz-Sabater, J., Nicolas, J., Peubey, C., Radu, R., Schepers, D., et al.: The ERA5 global reanalysis, Quarterly Journal of the Royal Meteorological Society, 146, 1999–2049, https://doi.org/https://doi.org/10.1002/qj.3803, 2020.

Hoskins, B. J. and Hodges, K. I.: A new perspective on Southern Hemisphere storm tracks, Journal of Climate, 18, 4108–4129, https://doi.org/https://doi.org/10.1175/JCLI3570.1, 2005.

Hu, Y., Rodier, S., Xu, K.-m., Sun, W., Huang, J., Lin, B., Zhai, P., and Josset, D.: Occurrence, liquid water content, and fraction of supercooled water clouds from combined CALIOP/IIR/MODIS measurements, Journal of Geophysical Research: Atmospheres, 115, https://doi.org/https://doi.org/10.1029/2009JD012384, 2010.

Huang, Y., Protat, A., Siems, S. T., and Manton, M. J.: A-Train observations of maritime midlatitude storm-track cloud systems: Comparing the Southern Ocean against the North Atlantic, Journal of Climate, 28, 1920–1939, https://doi.org/https://doi.org/10.1175/JCLI-D-14-00169.1, 2015.

https://doi.org/10.5194/egusphere-2023-518
Preprint. Discussion started: 11 April 2023

Huang, Y., Siems, S. T., Manton, M. J., Rosenfeld, D., Marchand, R., McFarquhar, G. M., and Protat, A.: What is the role of sea surface temperature in modulating cloud and precipitation properties over the Southern Ocean?, Journal of Climate, 29, 7453–7476, https://doi.org/https://doi.org/10.1175/JCLI-D-15-0768.1, 2016.

Kawai, H., Koshiro, T., and Webb, M. J.: Interpretation of factors controlling low cloud cover and low cloud feedback using a unified predictive index, Journal of Climate, 30, 9119–9131, https://doi.org/https://doi.org/10.1175/JCLI-D-16-0825.1, 2017.

Klein, S. A. and Hartmann, D. L.: The seasonal cycle of low stratiform clouds, Journal of Climate, 6, 1587–1606, https://doi.org/https://doi.org/10.1175/1520-0442(1993)006<1587:TSCOLS>2.0.CO;2, 1993.

Kolstad, E. W., Bracegirdle, T. J., and Seierstad, I. A.: Marine cold-air outbreaks in the North Atlantic: Temporal distribution and associations with large-scale atmospheric circulation, Climate dynamics, 33, 187–197, https://doi.org/https://doi.org/10.1007/s00382-007-0331-0, 2009.

Lang, F., Huang, Y., Siems, S., and Manton, M.: Characteristics of the Marine Atmospheric Boundary Layer Over the Southern Ocean in Response to the Synoptic Forcing, Journal of Geophysical Research: Atmospheres, 123, https://doi.org/https://doi.org/10.1029/2018JD028700, 2018.

Lang, F., Huang, Y., Protat, A., Truong, S., Siems, S., and Manton, M.: Shallow Convection and Precipitation Over the Southern Ocean: A Case Study During the CAPRICORN 2016 Field Campaign, Journal of Geophysical Research: Atmospheres, 126, e2020JD034 088, https://doi.org/https://doi.org/10.1029/2020JD034088, 2021.

Lang, F., Ackermann, L., Huang, Y., Truong, S. C., Siems, S. T., and Manton, M. J.: A climatology of open and closed mesoscale cellular convection over the Southern Ocean derived from Himawari-8 observations, Atmospheric Chemistry and Physics, 22, 2135–2152, https://doi.org/https://doi.org/10.5194/acp-22-2135-2022, 2022.

Mace, G. G., Zhang, Q., Vaughan, M., Marchand, R., Stephens, G., Trepte, C., and Winker, D.: A description of hydrometeor layer occurrence statistics derived from the first year of merged Cloudsat and CALIPSO data, Journal of Geophysical Research: Atmospheres, 114, https://doi.org/https://doi.org/10.1029/2007JD009755, 2009.

McCoy, I. L., Wood, R., and Fletcher, J. K.: Identifying Meteorological Controls on Open and Closed Mesoscale Cellular Convection Associated with Marine Cold Air Outbreaks, Journal of Geophysical Research: Atmospheres, 122, 11,678–11,702, https://doi.org/https://doi.org/10.1002/2017JD027031, 2017.

Minnis, P. and Harrison, E. F.: Diurnal variability of regional cloud and clear-sky radiative parameters derived from GOES data. Part I: Analysis method, Journal of Applied Meteorology, 23, https://doi.org/10.1175/1520-0450(1984)023

Morrison, A. E., Siems, S. T., and Manton, M. J.: A three-year climatology of cloud-top phase over the Southern Ocean and North Pacific, Journal of Climate, 24, 2405–2418, https://doi.org/https://doi.org/10.1175/2010JCLI3842.1, 2011.

Muhlbauer, A., McCoy, I. L., and Wood, R.: Climatology of stratocumulus cloud morphologies: microphysical properties and radiative effects, Atmospheric Chemistry and Physics, 14, 6695–6716, https://doi.org/https://doi.org/10.5194/acpd-14-6981-2014, 2014.

Naud, C. M., Booth, J. F., and Del Genio, A. D.: The relationship between boundary layer stability and cloud cover in the post-cold-frontal region, Journal of climate, 29, 8129–8149, https://doi.org/https://doi.org/10.1175/JCLI-D-15-0700.1, 2016.

Nicholls, S.: The dynamics of stratocumulus: Aircraft observations and comparisons with a mixed layer model, Quarterly Journal of the Royal Meteorological Society, 110, 783–820, https://doi.org/10.1002/qj.49711046603, 1984.

Papritz, L., Pfahl, S., Sodemann, H., and Wernli, H.: A climatology of cold air outbreaks and their impact on air–sea heat fluxes in the high-latitude South Pacific, Journal of Climate, 28, 342–364, https://doi.org/https://doi.org/10.1175/JCLI-D-14-00482.1, 2015.

https://doi.org/10.5194/egusphere-2023-518
Preprint. Discussion started: 11 April 2023

Rampal, N. and Davies, R.: On the Factors That Determine Boundary Layer Albedo, Journal of Geophysical Research: Atmospheres, 125, e2019JD032 244, https://doi.org/https://doi.org/10.1029/2019JD032244, 2020.

Trenberth, K. E. and Fasullo, J. T.: Simulation of present-day and twenty-first-century energy budgets of the southern oceans, Journal of Climate, 23, 440–454, https://doi.org/https://doi.org/10.1175/2009JCLI3152.1, 2010.

Truong, S., Huang, Y., Lang, F., Messmer, M., Simmonds, I., Siems, S., and Manton, M.: A climatology of the marine atmospheric boundary layer over the Southern Ocean from four field campaigns during 2016–2018, Journal of Geophysical Research: Atmospheres, 125, e2020JD033 214, https://doi.org/https://doi.org/10.1029/2020JD033214, 2020.

Watson-Parris, D., Sutherland, S., Christensen, M., Eastman, R., and Stier, P.: A Large-Scale Analysis of Pockets of Open Cells and Their Radiative Impact, Geophysical Research Letters, 48, e2020GL092 213, https://doi.org/https://doi.org/10.1029/2020GL092213, 2021.

Wood, R.: Stratocumulus clouds, Monthly Weather Review, 140, 2373–2423, https://doi.org/https://doi.org/10.1175/MWR-D-11-00121.1, 2012.

Wood, R. and Bretherton, C. S.: On the relationship between stratiform low cloud cover and lower-tropospheric stability, Journal of climate, 19, 6425–6432, https://doi.org/https://doi.org/10.1175/JCLI3988.1, 2006.

Wood, R. and Hartmann, D. L.: Spatial variability of liquid water path in marine low cloud: The importance of mesoscale cellular convection, Journal of Climate, 19, 1748–1764, https://doi.org/https://doi.org/10.1175/JCLI3702.1, 2006.

Yuan, T., Song, H., Wood, R., Mohrmann, J., Meyer, K., Oreopoulos, L., and Platnick, S.: Applying deep learning to NASA MODIS data to create a community record of marine low-cloud mesoscale morphology, Atmospheric Measurement Techniques, 13, 6989–6997, https://doi.org/https://doi.org/10.5194/amt-13-6989-2020, 2020.

https://doi.org/10.5194/egusphere-2023-518
Preprint. Discussion started: 11 April 2023

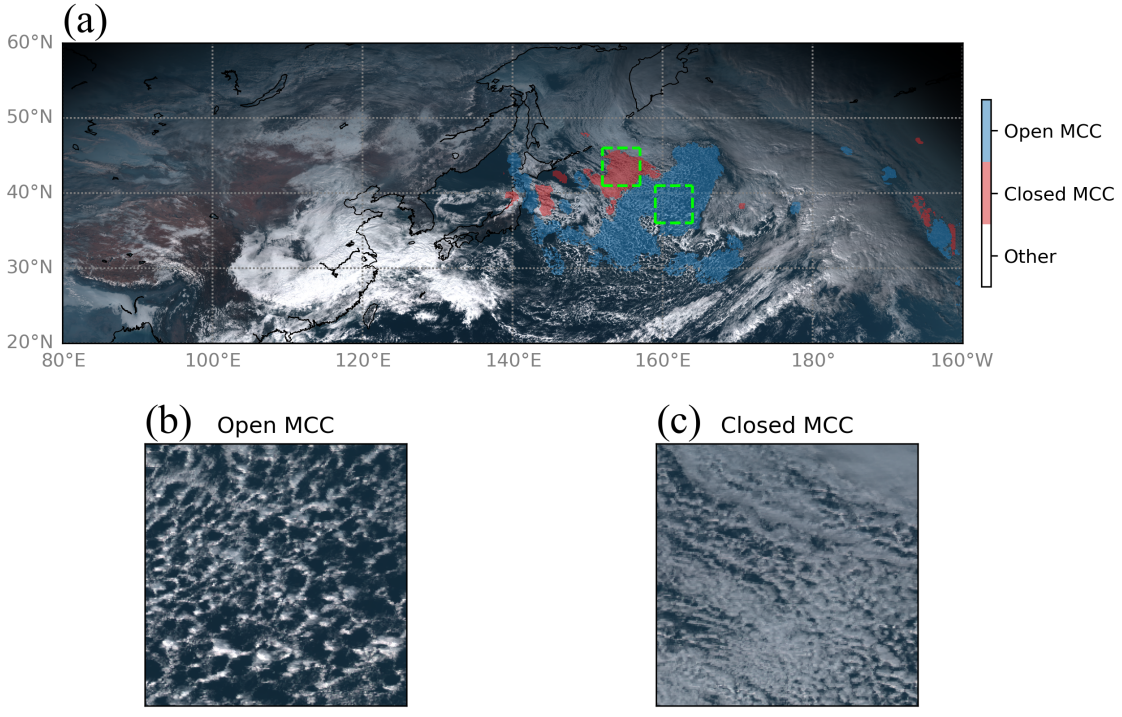

Figure 1. (a) An example scene of AHI Himawari-8 (visible) and MCC structures identified by the CNN on 7th January 2017 at 03:00 UTC. The green squares delimit the magnified area for the subscenes of (b) open and (c) closed MCC clouds.

https://doi.org/10.5194/egusphere-2023-518
Preprint. Discussion started: 11 April 2023

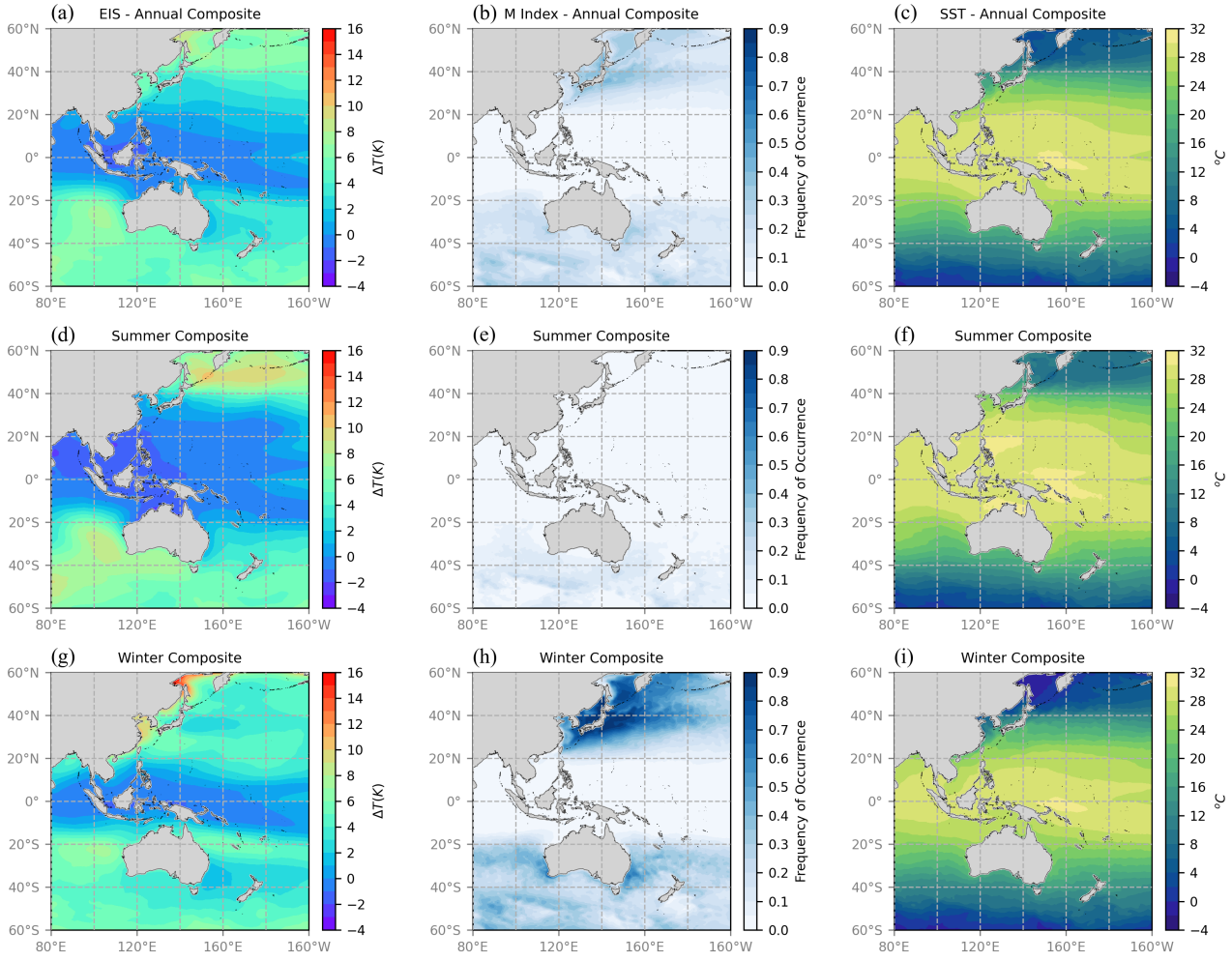

Figure 2. Annual mean (a-c), summer (d-f) and winter (g-i) seasons (2016-2018) for EIS, frequency of occurrence of M index for cases where M >0 K, and mean SST from ERA5 reanalysis products. Austral (boreal) summer is defined by December-February (June-August), while austral (boreal) winter is defined by June-August (December-February).

https://doi.org/10.5194/egusphere-2023-518
Preprint. Discussion started: 11 April 2023

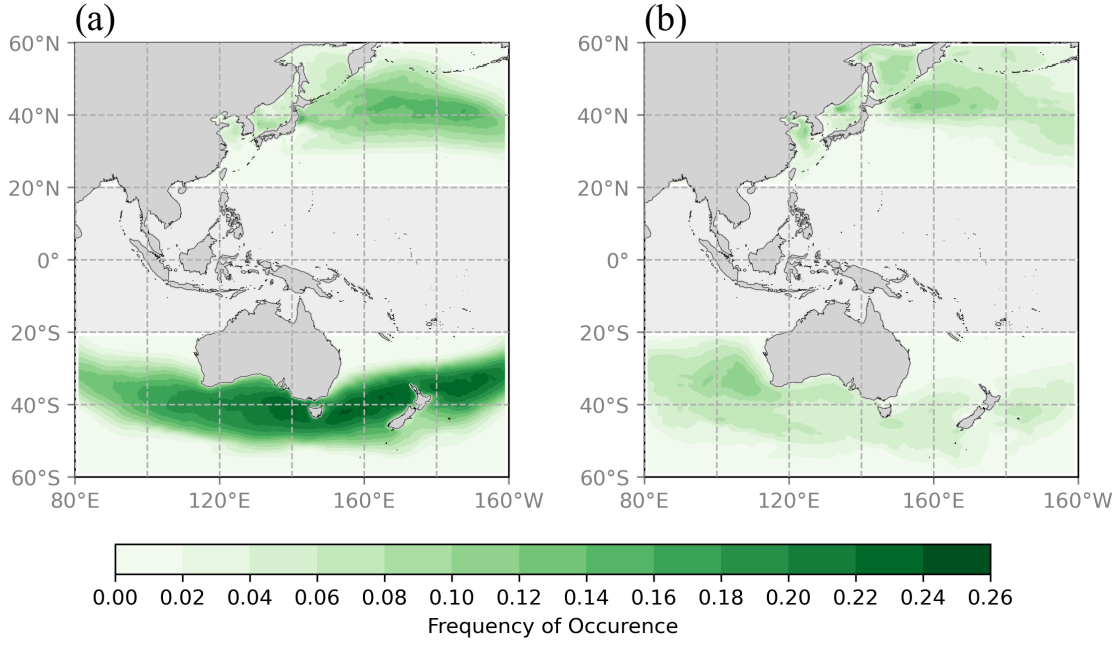

Figure 3. Distribution of the annual frequency of occurrence of the MCC clouds for the period 2016-2018. (a) Open MCC and (b) closed MCC structures.

https://doi.org/10.5194/egusphere-2023-518
Preprint. Discussion started: 11 April 2023

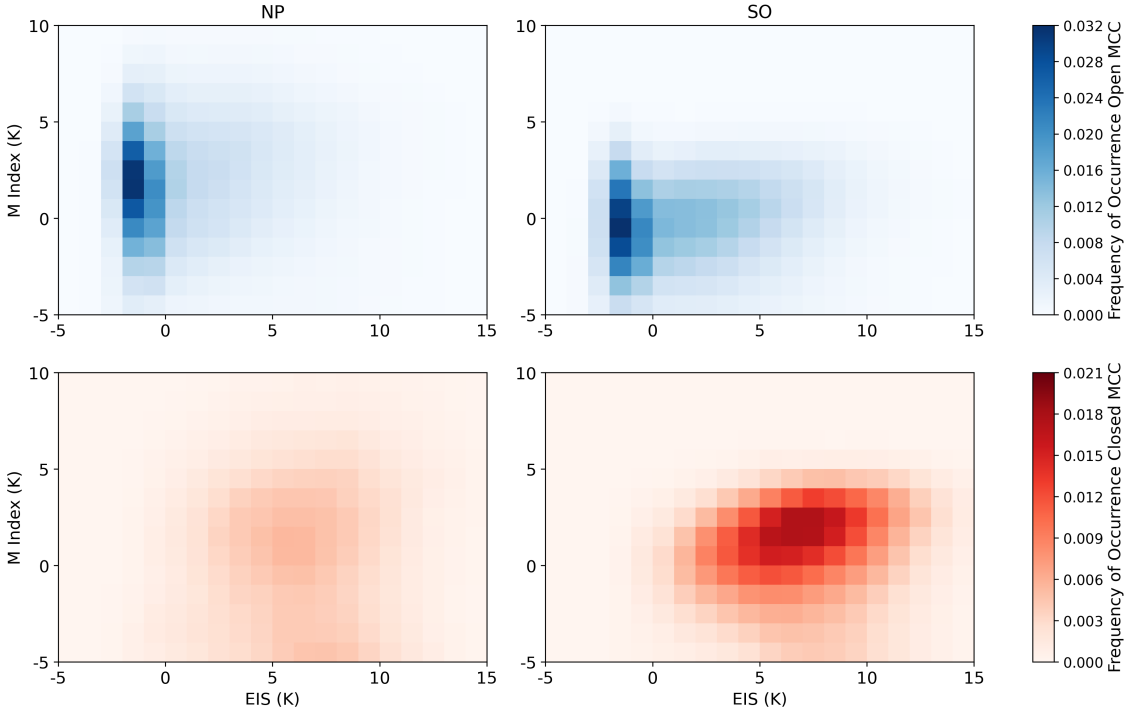

Figure 4. Two-dimensional composite histograms of M index and EIS for open (top row) and closed (bottom row) MCC clouds for the period 2016-2018. Data is for both NP (left column) and SO (right column) regions.

https://doi.org/10.5194/egusphere-2023-518
Preprint. Discussion started: 11 April 2023

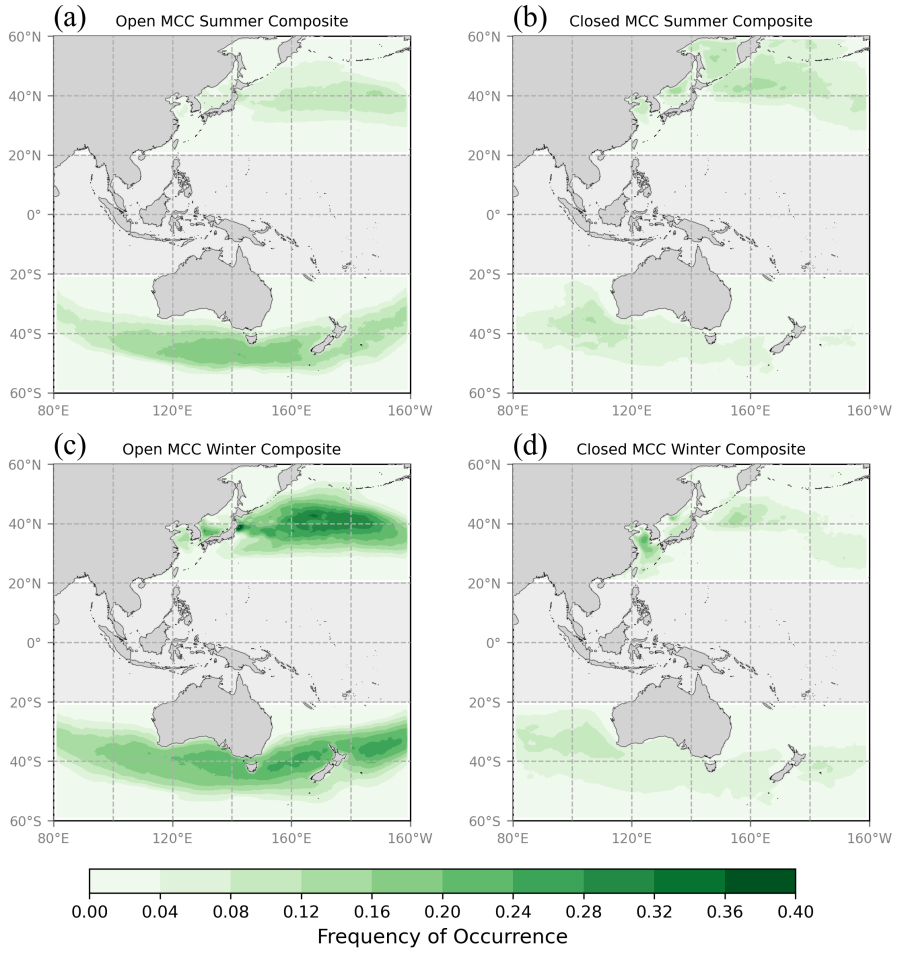

Figure 5. Summer and winter composites of the frequency of occurrence of MCC clouds for the period 2016-2018. (a,b) Boreal and austral summer together on the same plots and (c,d) boreal and austral winter together on the same plots. Austral (boreal) summer is defined by December-February (June-August), while austral (boreal) winter is defined by June-August (December-February).

https://doi.org/10.5194/egusphere-2023-518
Preprint. Discussion started: 11 April 2023

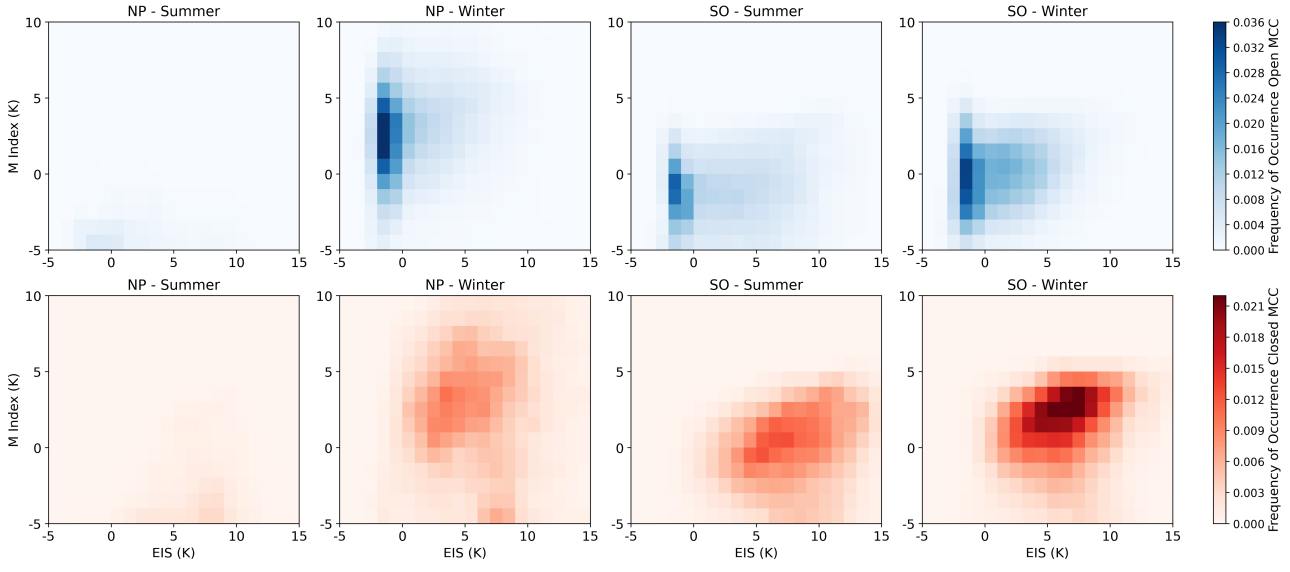

Figure 6. Seasonal two-dimensional composite histograms of M index and EIS for open and closed MCC clouds for the period 2016-2018. Data is for both NP (left two columns) and SO (right two columns) regions. Austral (boreal) summer is defined by December-February (June-August), while austral (boreal) winter is defined by June-August (December-February).

https://doi.org/10.5194/egusphere-2023-518
Preprint. Discussion started: 11 April 2023

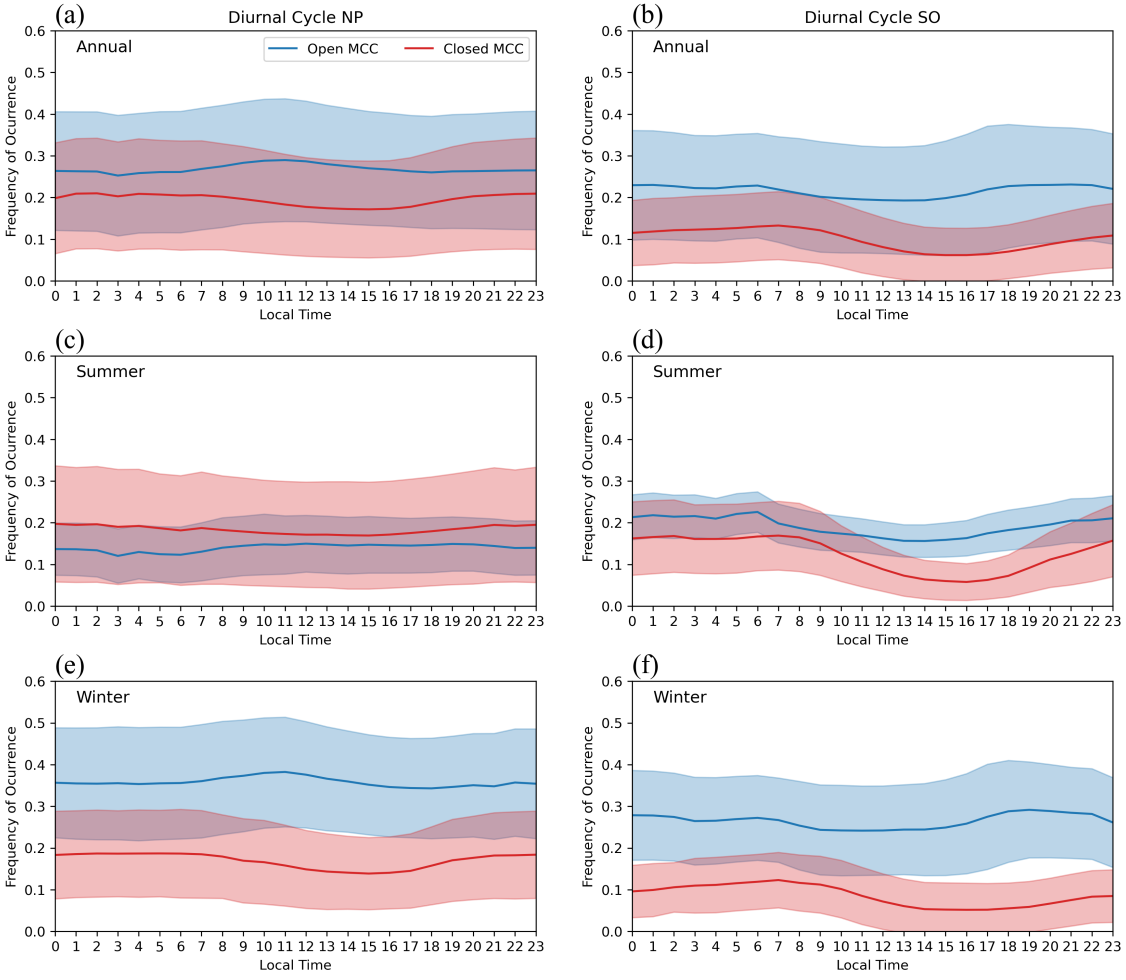

Figure 7. Diurnal cycle of the frequency of occurrence of MCC structures for the period 2016–2018. Shown are open MCC (blue) and closed MCC (red) structures. The diurnal cycle is calculated over boxes of 10 × 10°, center at 40°N, 170°W and 45°S, 130°W. Seasonal means are shown for summer and winter. Shadings represent 1 standard deviation. Frequencies are calculated for the latitudinal band between 40 and 50° for both hemispheres.

https://doi.org/10.5194/egusphere-2023-518
Preprint. Discussion started: 11 April 2023

Table 1. Seasonal means (standard deviation) of estimated inversion strength (EIS) and M index. Austral (boreal) summer is defined by December-February (June-August), while austral (boreal) winter is defined by June-August (December-February).

Region	Season	Open MCC		Closed MCC	
		EIS (K)	M Index (K)	EIS (K)	M Index (K)
NP	Summer	7.7 (1.8)	-11.9 (2.3)	9.0 (1.8)	-11.4 (2.5)
	Winter	2.3 (1.5)	3.5 (1.3)	6.9 (2.2)	3.1 (2.6)
SO	Summer	4.7 (1.6)	-2.5 (1.8)	8.6 (1.9))	-2.4 (2.5)
	Winter	2.6 (0.9)	0.9 (0.9)	7.1 (1.5)	1.6 (1.2)